Experimental Analyses of Vibration and Noise of Faulted Planetary Gearbox

Zhuang Li

McNeese State University, USA

e-mail: zli@mcneese.edu

ABSTRACT

Epicyclic gear trains are widely used in various industrial sectors due to their advantages over fixed-axis gears, such as high torque capability, compact size, differential and planetary designs, ease of adjusting gear ratios and even directions of rotation. This research focuses on planetary gearbox whose degree of freedom is one. The geometry and dynamics of the planetary gear train are quite complicated compared with the fixed-axis gear train. In an earlier research, three theoretical models for faulted sun, planet, and ring gears were analyzed and the signature frequencies of the three cases were derived. In this paper, experiments were conducted on a Drivetrain Diagnostics Simulator with various faults of the sun gear in order to verify the previously proposed theoretical models. Both the vibration and noise signals were collected and analyzed using signal processing techniques in the time and frequency domains. The sidebands around gear mesh frequency due to the fault signature frequencies are also discussed accordingly. The signals of healthy and faulted gear trains were also compared carefully. The existence of the signature frequency can be used to detect mechanical defects and prevent catastrophic consequences.

Keywords: planetary gearbox, fault diagnosis, signature frequency
I-INCE Classification of Subjects Number(s): 11.1, 74.5

1. INTRODUCTION

Gear trains can be classified into three categories.

(1) *Fixed-axis (or fixed-shaft) gear train*. All shafts are fixed in space. Therefore, every gear's speed is with respect to ground or zero.

(2) *Epicyclic gear train*. One or more gear axis also rotates in space. So the absolute speed of a gear is the relative speed with respect to the shaft plus the shaft's speed with respect to ground. Based on the number of degrees of freedom, the epicyclic gear trains can be further categorized as differential and planetary gear trains. The differential mechanism is commonly used in the rear axle shaft of an automobile. Planetary gears are widely used in heavy duty power transmission such as helicopter and agricultural equipment because of their high torque capability but in compact sizes.

(3) *Compound gear train*: a combination of fixed-axis and epicyclic gear trains.

This paper focuses on planetary gear trains.A planetary gear train consists of four components: sun gears whose axes are fixed axes, a carrier (also called arm) which rotates in space about the fixed axes, planet gears which rotate along with the carrier, and frame and bearings. Levai identified 12 possible variations of planetary gear trains (1). A planetary gear train has one and only one carrier which supports one or more planets. All sun gears and the carrier rotate about the same axis. Large speed reduction/torque increase can be obtained in a compact design. For certain planetary gear trains, adjusting the number of teeth of a gear may change the gear ratio significantly as well as the rotation direction.

From the condition monitoring and fault diagnosis perspectives, many researchers have done excellent work in the last a couple of decades. Samuel and Pines did a thorough review on gear fault detection based on vibration techniques (2). For planetary gears particularly, McFadden and Smith explained the asymmetry of the sidebands about the meshing frequency by using the phase modulations (3). Parker also derived a forcing model to study the planet phasing and its effects on

planetary gearbox vibration (4). Vicuna derived the same conclusions as McFadden and Smith using the Fourier analysis (5). In his PhD dissertation, Inalpolat proposed a simplified mathematical model on sidebands where he considered the amplitude modulation caused by the carrier rotation and the effects of various configuration parameters (6). Feng and Zuo further considered both the amplitude and frequency modulations and presented a sophisticated model for fault diagnosis (7).

The author derived the signature frequencies for faulted sun, planet, and ring gears (8). This paper will be more extended experimental investigations based on the theoretical models developed in reference (8). In this paper, some fundamentals and the three signature frequency calculations are briefly reviewed in Section 2. Section 3 is on experimental setup. Results will be presented along with discussions in Section 4. This paper will be completed by the conclusion section.

2. FUNDAMENTALS

Figure 1 illustrates the type of planetary gearbox studied in this paper, one of the most basic planetary gearbox configurations. The input is a sun gear which meshes with planet gears supported by the carrier. The number of planets is denoted by K. The number of planet and tooth numbers all determine the planet phasing. The planets also mesh with a fixed ring gears ($\omega_3 = 0$). The output is the floating carrier. As the configuration is symmetric, Figure 1 only illustrates half of the configuration.

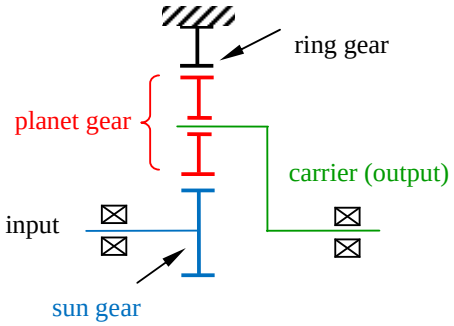

Figure 1. Planetary gear configuration under study

Let N_1, N_2, N_3 be the numbers of teeth of the sun, planet, and ring gears, and ω_1 the input sun gear's angular speed. Then, for such a configuration, the absolute speeds of carrier and planet are

$$\omega_c = \frac{\omega_1 N_1}{N_1 + N_3}, \text{ and } \omega_2 = -\frac{\omega_1 N_1}{2N_2}. \quad (1)$$

It can be seen that the carrier rotates in the same direction as the input sun gear but with a slower speed, while the planet rotates in the opposite direction designated by the negative sign. In addition, the mesh frequency is given by

$$\omega_m = \frac{N_1 N_3}{N_1 + N_3}\omega_1 = N_3 \omega_c. \quad (2)$$

Reference (8) derived the signature frequencies for faulted sun, planet, and ring gears based on the assumption that a faulted tooth with reduced stiffness will cause a series of impacts. Such a signal will be transmitted through various paths to the sensors. One path is through the input sun gear → input shaft → bearing → bearing housing → sensor. In this case, the distance between the impact source and the sensor is constant since the input shaft is fixed in space. Another path is through the planet gear → ring gear → case → sensor. Since the planet gear is moving in space with the carrier, the path distance varies which causes amplitude modulation.

For each faulted gear, the time interval between two adjacent impacts was derived using gearbox configuration geometry and dynamics. The fault signature frequencies are thus calculated. The formulas are summarized in Table 1, where the subscripts represent "faulted sun", "faulted planet", and "faulted ring", respectively.

It is worth mentioning that the transmission paths explained above are for vibrations. In the meantime, when such a vibration is transmitted to the structure, such as bearing housing, rotor deck, casing, etc., the energy is spread over larger surface areas which generate sound. Therefore, a microphone is used in this study to measure sound as sound also includes the information of gear rotations.

Table 1. Time intervals and signature frequencies of faulted planetary gearbox cases

Case	Signature Frequency	Time Between Impacts
faulted sun gear	$\omega_{FS} = \frac{KN_3\omega_1}{N_1+N_3} = \frac{KN_3\omega_c}{N_1}$	$\Delta T_{FS} = \frac{2\pi}{K\left(\omega_1-\omega_c\right)}$
faulted ring gear	$\omega_{FR} = K\omega_c = \frac{KN_1\omega_1}{N_1+N_3}$	$\Delta T_{FR} = \frac{2\pi}{K\omega_c}$
faulted planet gear	$\omega_{FP} = \frac{2N_3\omega_c}{N_2} = \frac{N_1N_3\omega_1}{N_2\left(N_1+N_2\right)}$	$\Delta T_{FP} = \frac{\pi N_2}{N_3\omega_c}$

3. Experimental setup

Experiments were conducted on the Drivetrain Dynamics Simulator (DDS). It consists of one-stage planetary gear and a two-stage spur gearbox. The DDS, as shown in Figure 2, is driven by a 3-phase 3 HP induction motor controlled by a VFD (variable frequency drive). The planetary gearbox has a 28-tooth sun gear (N_1 = 28), four 36-tooth planets (K = 4, N_1 = 2836), a 100-tooth ring gear (N_3 = 100). All gears are standard module 1 gears. The floating carrier is the output. The assembly drawing is also included in Figure 2 to illustrate more detailed configuration. The carrier shaft is used to drive the two-stage spur gearbox. The module is 1.5, and the two stage gear ratios are 100:29 and 90:36, respectively. The DDS is also equipped with a magnetic load brake which provides torsional loading to the system. Based on the information, some important parameters are calculated in Table 2.

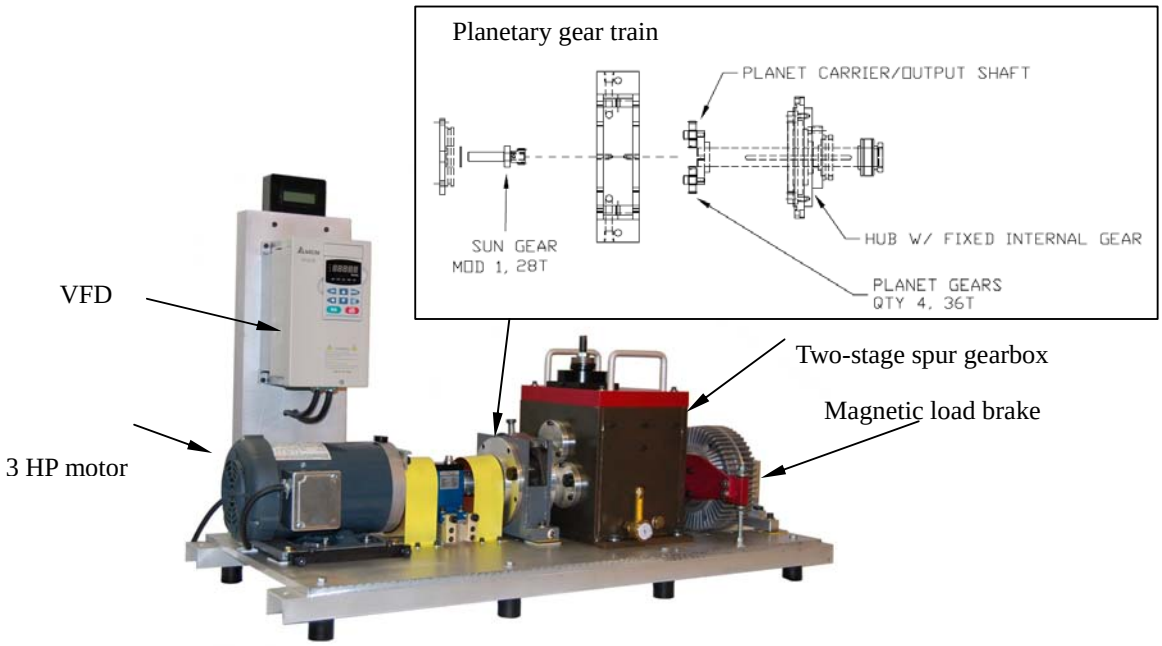

Figure 2. Drivetrain Dynamics Simulator

Table 2. Important parameters of the DDS

gear ratio	$r = \frac{\omega_1}{\omega_c} = \frac{N_1 + N_3}{N_1} = \frac{28+100}{28} = 4.571$
sun fault signature frequency	$\omega_{FS} = \frac{KN_3\omega_1}{N_1 + N_3} = \frac{4\times100\times\omega_1}{28+100} = 3.125\omega_1$
mesh frequency (planetary gearbox)	$\omega_m = \omega_1 \frac{N_1 N_3}{N_1 + N_3} = 21.875\omega_1$
mesh frequency (first stage spur gearbox)	$\omega_{s1} = 6.344\omega_1$
mesh frequency (second stage spur gearbox)	$\omega_{s2} = 2.284\omega_1$

A PCB U352 C68 accelerometer was mounted on the top of the planetary gearbox to measure the vibration, as illustrated in Figure 3. A PCB 377B02 microphone powered by the preamplifier model 426E01 is used to measure the sound pressure levels. The microphone is a free-field one, so it faces directly to the gearbox with a distance of 0.5 metre. Data acquisition was performed using LabVIEW with the data acquisition card NI PCI-4472. The data acquisition device provides IEPE power supply to both the accelerometer and preamplifier 426E01. All sensors can connected to the data acquisition board using standard BNC-SMA cables. Both the acceleration and sound signals are sampled with AC coupling which removes the DC offset.

Figure 3. Accelerometer mounted on the gearbox to measure vibration signals.

Three sun gears, an intact and two faulted, were tested in order to investigate the theoretical model presented in Section 2. Figure 4 illustrates these three gears under test. The intact gear serves as the reference specimen and baseline data were collected for comparison purposes. The second one has only one chipped tooth. So it causes impacts with every planet gear consecutively as the sun gear rotates faster than the carrier. Since there is only one faulted tooth, the energy caused by impacts is relatively low. Additionally, when the chipped tooth is engaged with a planet, although it does cause an impact, because three more healthy teeth are engaged with the other three planets, such high vibration will be somehow distributed over the planets. This is in fact an advantage of the design of planetary gearbox, but gives challenges to fault diagnosis.

Type (c) is a gear with surface fault. All the teeth are manually scratched to introduce surface deterioration. Notice in the figure that the gray area near the top of each tooth is the deteriorated surface. As all the teeth of type (c) are faulted, they contribute impact vibrations to the system more often than the one with chipped tooth. Presumably, the vibration energy will be greater and the induced fault frequency's amplitude will be higher.

Each gear was tested at three speeds: 1200 rpm, 1500 rpm, and 1800 rpm. In addition, at each speed, three load conditions were simulated: light, medium, and high controlled by the magnetic break.

(a) (b) (c)

Figure 4. Sun gears used in experimental investigations:
(a) intact gear, (b) gear with a chipped tooth, (c) gear with surface fault.

4. EXPERIMENTAL RESULTS AND DISCUSSIONS

As explained above, totally 27 measurements were carried out. Each measurement includes both the vibration and sound signals. Also, each signal consists of quite a few frequency components of interest. Considering the limited space, not all the data analyses are reported in this paper. Instead, tables and charts will be utilized to help visualize the comparisons.

4.1 Overall vibration amplitudes and sound pressure levels

The simplest condition monitoring technique is the trends of the overall vibration and acoustic amplitudes. Table 3 lists all the vibration amplitudes (*g* rms) and sound pressure levels (dB) for the 27 measurements. Some observations can be concluded as follows.

- For a specific sun gear, an increase in load does not necessarily increase the vibration or sound overall levels, although a rough trend exists.
- For a specific sun gear, an increase in rotating speed does not necessarily increase the vibration or sound overall levels.
- Compared the intact with surface faulted gear, for all the speed and load conditions, the faulted one has higher vibration and acoustic amplitudes. This agrees with the analysis above.
- However, compared with the intact with chipped-tooth-gear, the faulted gear does not necessarily increase the vibration or acoustic amplitude. On the contrary, out of the 18 comparisons (9 vibration comparisons and 9 acoustic comparisons), 16 of them show that the chipped-tooth-gear has even lower amplitudes than the intact one.

Table 3. Overall vibration amplitudes and sound pressure levels

speed (rpm)	**gear type**	**light load**		**medium load**		**high load**	
		vibration (*g* rms)	SPL (dB)	vibration (*g* rms)	SPL (dB)	vibration (*g* rms)	SPL (dB)
1200	intact	0.0488	71.2	0.0788	71.2	0.0873	71.7
	chipped tooth	0.0663	70.7	0.0741	70.8	0.0817	71.5
	surface fault	0.139	73.2	0.175	74.6	0.206	75.5
1500	intact	0.0881	74.1	0.105	73.3	0.111	73.7
	chipped tooth	0.0808	72.6	0.0803	72.2	0.0858	71.8
	surface fault	0.176	75.9	0.289	79.5	0.327	79.6
1800	intact	0.086	74.8	0.113	74.3	0.124	74.6
	chipped tooth	0.0979	72.6	0.107	73.4	0.115	72.9
	surface fault	0.327	77.5	0.286	78.4	0.316	78.8

4.2 Time waveforms

The time waveform is also a straightforward data presentation used to visualize the basic nature of the signal and to check the existence of transient components. Figure 5 compares the three cases for the 1200 rpm and light loading condition. It can be seen from the figure that the intact gear also create some impact-type signals although their amplitudes are not much greater than regular vibration. However, the chipped tooth causes significant individual impacts and their amplitudes are much higher. The surface faulted gear, on the other hand, increases the overall vibration amplitude, but the increase is in a broad band because every tooth is faulted.

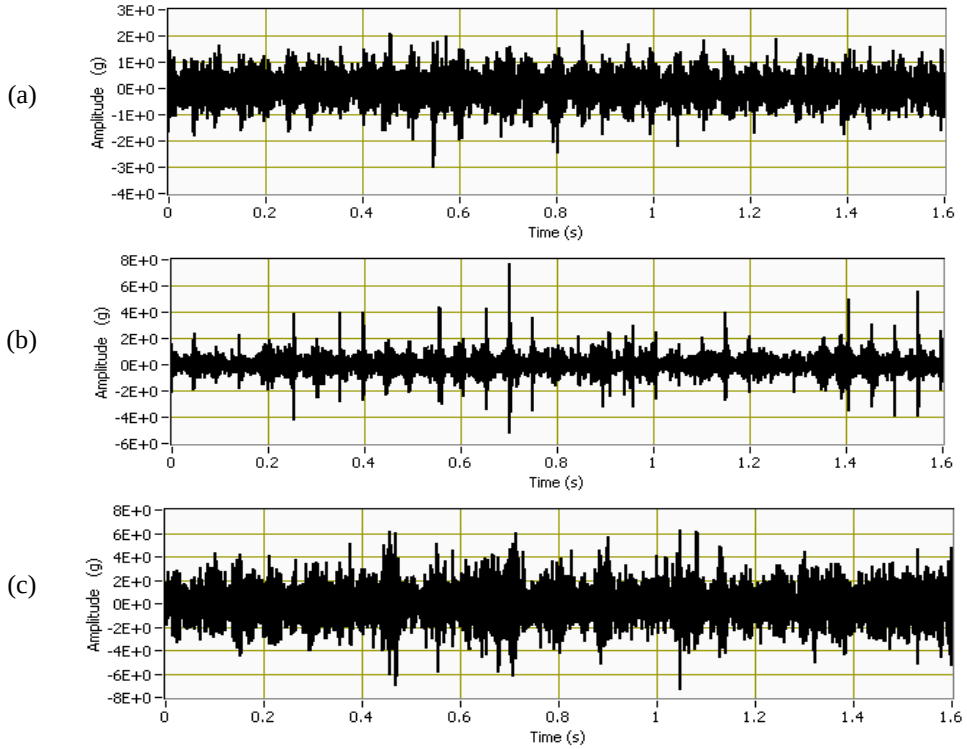

Figure 5. Comparison of time waveforms at 1200 rpm under light loading condition: (a) intact gear, (b) gear with a chipped tooth, (c) gear with surface fault.

4.3 Comparisons of fault-related frequencies

More detailed comparisons must be carefully done in the frequency domain which involves all the fault-related frequency components. The impacts caused by a faulted tooth follow certain time interval and possess a signature frequency as explained in Section 2. For example, using the second formula in Table 2, if the input speed is 1200 rpm, then the signature frequency is $f_{FS} = 3.125 \times 1200 / 60 = 62.5$ Hz. Figure 6 show the spectra of the three sun gears at 1200 rpm under light loading condition. It can be seen that at 62.5 Hz there is a slight increase from baseline to the chipped tooth spectrum, and a major increase from baseline to the surface faulted one.

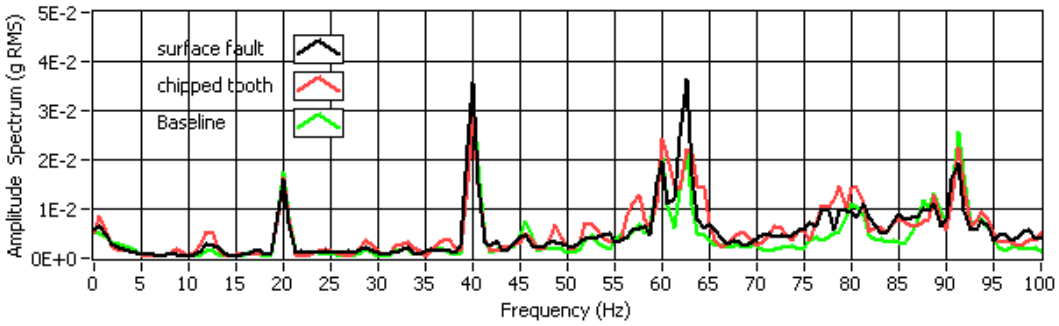

Figure 6. Spectral comparison for the three cases at 1200 rpm, light load condition

It will be impractical to show all the spectra and analyze their frequency contents. In this paper only six frequency components are compared:

ω_1 – input shaft frequency
ω_{FS} – signature frequency of faulted sun gear, calculated using $\omega_{FS} = 3.125\ \omega_1$
$\omega_m \pm \omega_{FS}$ and $\omega_m \pm 2\omega_{FS}$ – sidebands around the tooth mesh frequency

Figure 7 through Figure 9 compare these frequency components' amplitudes. The left column is vibration signals in *g* rms, while the right column is sound pressure in Pa rms. Sub-figures (a) through (c) are vibration channels for light, medium, and high loading conditions; figures (e) through (f) are sound channels accordingly. All the sound signals don't have clear ω_1 components, so they are not included in the right column comparisons. Some observations can be concluded as follows.

- For a given sun gear at a specific speed, the increase in load does not vary the ω_1 amplitude much.
- The introduction of tooth fault does not necessarily increase the amplitudes of these fault-related components.
- The surface faulted gear typically has higher amplitudes than the chipped-tooth gear.

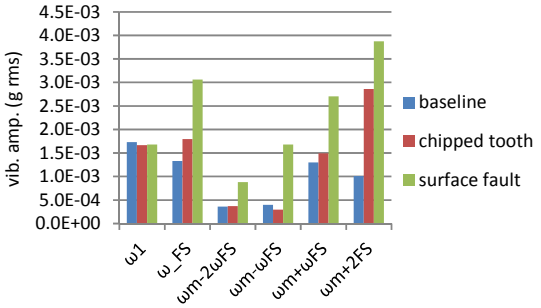

(a) light load

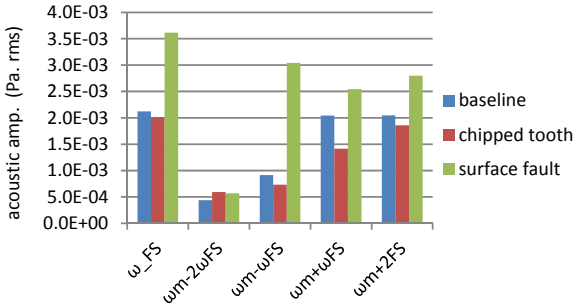

(d) light load

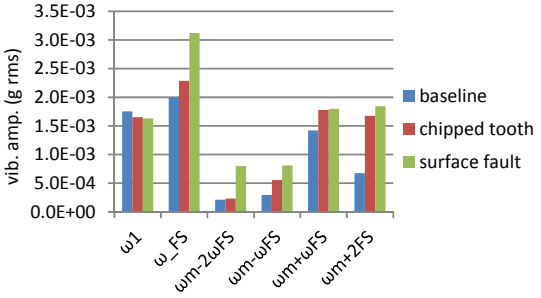

(b) medium load

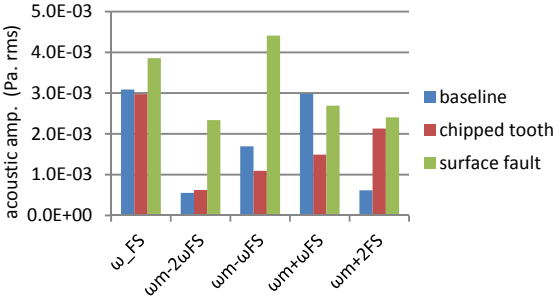

(e) medium load

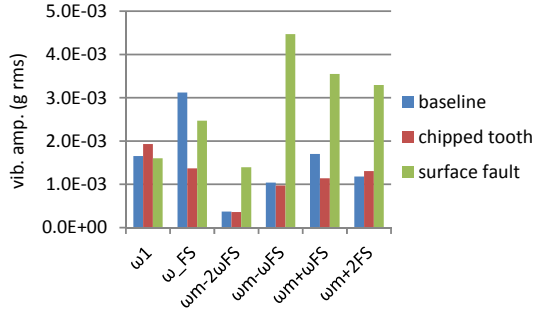

(c) high load

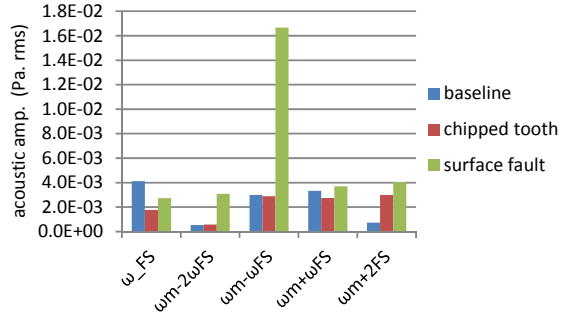

(f) high load

Figure 7. Comparison of fault-related frequencies for 1200 rpm input speed.

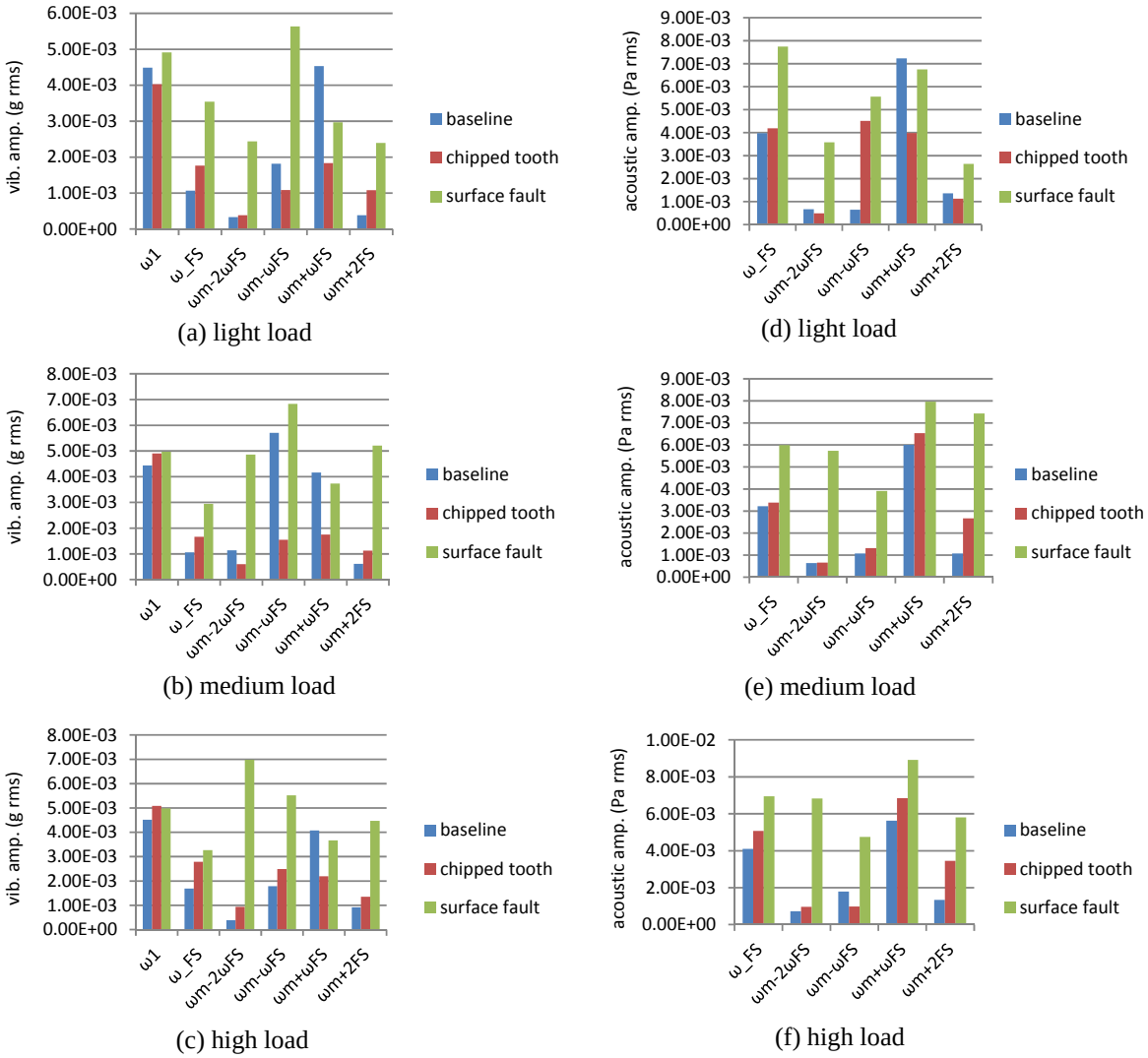

Figure 8. Comparison of fault-related frequencies for 1500 rpm input speed

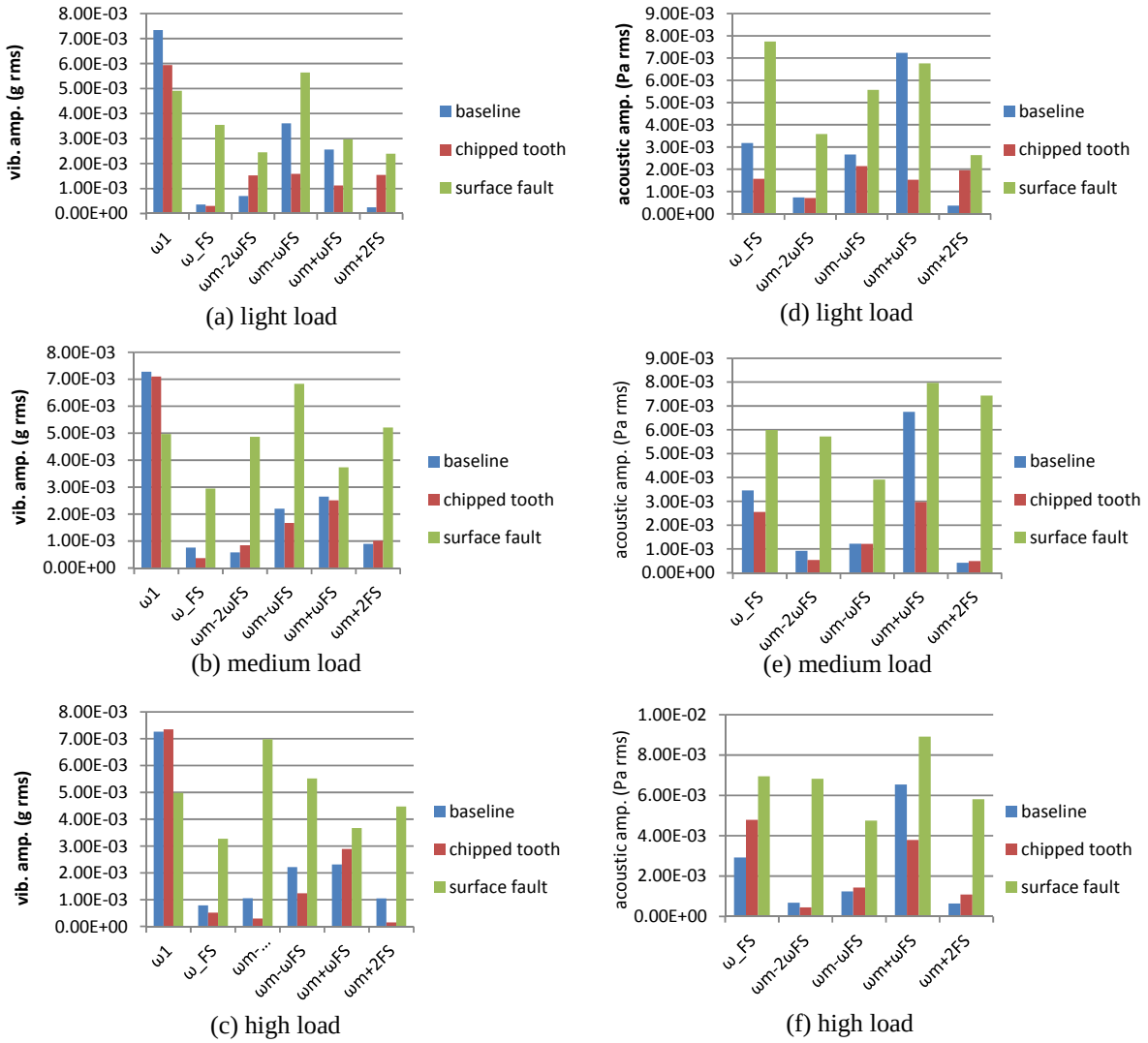

Figure 9. Comparison of fault-related frequencies for 1800 rpm input speed

4.4 Using the rms value of fault-related frequencies

From the three figures above it can be seen that although five fault-related frequencies are compared, not an individual one can serve as the index for fault diagnosis purpose. Instead, the square root of the square sum of these amplitudes (rms) may serve as a single-value objective index. A significant increase in such an index indicates the occurrence of a fault.

$$A_{index} = \sqrt{\sum_i A_i^2}\,, \tag{3}$$

where each A_i is the amplitude of a fault-related frequency. If all these components are comprehensively considered using Eq. (3), then the calculated indices are listed in Table 4. Different than Table 3 where 16 values of chipped-tooth gear are lower than those of the intact gear, only four comparisons (highlighted in yellow) did not show the increase in amplitude in chipped-tooth gear. Also three out of these four are sound signals. So the accuracy is improved, especially in the vibration signals.

Table 4. Fault diagnosis using the rms value of fault-related frequencies

speed (rpm)	gear type	light load		medium load		high load	
		vibration (*g* rms)	sound (Pa rms)	vibration (*g* rms)	sound (Pa rms)	vibration (*g* rms)	sound (Pa rms)
1200	intact	2.18E-03	4.16E-03	2.57E-03	5.17E-03	1.48E-02	6.77E-03
	chipped tooth	3.72E-03	4.53E-03	3.40E-02	7.31E-03	1.73E-02	6.97E-03
	surface fault	5.94E-03	8.03E-03	4.20E-02	2.26E-02	1.89E-02	5.34E-02
1500	intact	1.48E-02	2.24E-02	9.79E-03	1.03E-02	7.22E-03	1.10E-02
	chipped tooth	2.11E-02	1.50E-02	5.66E-03	1.10E-02	7.41E-03	1.14E-02
	surface fault	6.37E-02	3.96E-02	1.26E-01	1.91E-02	1.39E-01	2.00E-02
1800	intact	5.49E-03	8.38E-03	5.96E-03	7.76E-03	7.62E-03	7.33E-03
	chipped tooth	1.46E-02	3.70E-03	1.33E-02	5.65E-03	1.51E-02	7.79E-03
	surface fault	6.37E-02	1.25E-02	1.26E-01	1.42E-02	1.39E-01	1.52E-02

5. CONCLUSIONS

This paper is mainly an experimental investigation for fault diagnosis of a planetary gearbox. The theoretical models, however, are reviewed and explained. 27 measurements were conducted with three sun gears (one intact and two faulted) at three input speeds under three loading conditions. The fault in the chipped-tooth gear is very small to be detected. All the teeth of the surface faulted gear have surface defects, so the vibration energy associated with fault is much stronger. Overall vibration and sound amplitudes and time waveforms are briefly compared. Then five fault-related frequencies are compared in details. Some observations are reported. Finally, a single-value which comprehensively includes all the fault-related frequencies is proposed as the fault diagnosis index which increased the detection accuracy.

REFERENCES

1. Zoltan Levai, Theory of Epicyclic Gears and Epicyclic Change-Speed Gears, Budapest, 1966.
2. Paul D. Samuel, Darryll J. Pines, A review of vibration-based techniques for helicopter transmission diagnostics, Journal of Sound and Vibration, **282**(1-2), 475-508, 2005
3. P. D. McFadden and J. Smith, An explanation for the asymmetry of the modulation sidebands about the tooth meshing frequency in epicyclic gear vibration, Proceedings of the Institution of Mechanical Engineering, 199(C1), pp 65–70 , 1985
4. Robert Parker, A Physical Explanation for the Effectiveness of Planet Phasing to Suppress Planetary Gearbox Vibration, Journal of Sound and Vibration, **236**(4), 561-573, 2000
5. C. M. Vicuña, Theoretical frequency analysis of vibrations from planetary gearboxes, Forsch Ingenieurwes. 76, pp.15–31, 2012
6. Murat Inalpolat, A Theoretical and Experimental Investigation of Modulation Sidebands of Planetary Gear Sets, PhD dissertation, Ohio State University, 2009
7. Zhipeng Feng, Ming J. Zuo, Vibration Signal Models for fault Diagnosis of Planetary Gearboxes, Journal of Sound and Vibration, **331**, 4919-4939, 2012
8. Zhuang Li, Daniel Rangel, Philip Hedlesky, Ethan Leger, A study of vibration characteristics of planetary gear trains, Proceedings of the 21st International Congress of Sound and Vibration, Beijing, July 13~17, 2014